MODELING OF AXIALLY LOADED HSS SLENDER STEEL MEMBERS RETROFITTED WITH COMPOSITES

Amr Shaat, Waleed Safwat El Sayed Fahmy and Amir Fam
Department of Civil Engineering, Queen's University, Kingston, Ontario, Canada
E-mail: fam@civil.queens.ca

Abstract

This paper describes an analytical model developed to predict the behaviour of axially loaded slender members composed of steel hollow structural sections (HSS), retrofitted with carbon-fibre reinforced polymer (CFRP) composite sheets. A previous experimental study by the authors showed that gain in strength due to CFRP retrofitting was highly sensitive to the specimen's imperfection. As such, developing an analytical model was necessary to uncouple the effects of imperfection and number of CFRP layers. The model predicts the load versus axial and lateral displacements, and accounts for steel plasticity, the built-in through-thickness residual stresses, geometric non-linearity, including initial imperfection, and the contribution of CFRP sheets. The model was verified against results of the experimental program and showed reasonable agreement. The model was then used in a parametric study. The study demonstrated that retrofitting slender HSS columns using CFRP sheets increased both the axial strength and stiffness substantially.

Introduction

The progressive aging and deterioration, combined with the requirements for higher load capacity, results in an increase in the number of bridges which do not meet the current code standards. Conventional retrofitting techniques for steel members, in general, involve bolting or welding additional steel plates. These techniques have a number of shortcomings, including the added self weight of steel plates, the installation time, and the need for an elaborate and expensive shoring system. Fiber-reinforced polymers (FRP) are rapidly gaining acceptance as an effective material for retrofitting a wide range of structures, particularly due to their excellent corrosion resistance and fatigue properties (Hollaway and Cadei, 2002 and Shaat et al., 2004).

The majority of applications of these materials, so far, have been flexural members such as beams and bridge girders where bonding of FRP on the tension side is very effective in upgrading the structural performance of such members. Nevertheless, the failure mode of axially loaded steel members such as columns or truss members with medium to high slenderness ratios is generally governed by overall buckling, which is essentially a flexural problem. Therefore, bonding FRP sheets or strips of adequate stiffness in the longitudinal direction of slender members could be quite effective.

An experimental study was performed (Shaat and Fam, 2006) to investigate the effect of adhesively bonded carbon-FRP (CFRP) sheets on the behaviour of axially loaded HSS columns. The column's cross sectional shape is shown in Fig. 1(a) and the column length was 2380 mm, such that slenderness ratio was 68. In slender columns, where overall buckling governs, it is anticipated that the ultra-high modulus CFRP sheets would contribute to the flexural stiffness of the column, and at large deflections, may resist some tension on the outer surface. It was shown experimentally that CFRP sheets have indeed increased the columns' strengths by up to 23 percent. The study, however, revealed the sensitivity of axially loaded slender columns to their inherent geometric out-of-straightness and alignment (imperfections), which affects both the ultimate strength and stiffness of the specimens. Residual stresses are also an important factor, which can affect the behaviour of cold-formed sections. While the major parameter intended in the experimental investigation was the effect of number of CFRP layers, it is believed that geometric imperfections have also varied among the specimens. As such, no specific correlation could be established between the amount of strength gain and the amount of CFRP.

M. Pandey et al. (eds), Advances in Engineering Structures, Mechanics & Construction, 227–238.

A theoretical study including finite element analysis and analytical modeling is being developed by the authors to assess the exclusive contribution of CFRP sheets to the strength and stiffness of slender HSS steel members and understand their behaviour. The objective of this paper, which is the first phase in the analytical program, is to introduce a simplified analytical model to predict the load versus axial and lateral displacement responses of axially loaded HSS members retrofitted with CFRP. It is anticipated that further refinement of this approach will be needed in the future. The model is verified using the experimental results and is used to uncouple the effect of geometric imperfections from the effect of CFRP retrofitting. In the following sections, a brief summary of the experimental research program is given, followed by a detailed description of the analytical model. The model verification, using the experimental load-lateral displacement, load-axial displacement and load-axial strain responses, is then presented. Finally, the parametric study is presented.

Summary of Experimental Investigation

A brief summary of the experimental study is presented in this section, whereas more details can be found elsewhere (Shaat and Fam 2006). The experimental study included 5 axial compression tests, conducted on a standard 89 x 89 x 3.2 mm HSS section (Fig. 1(a)) with nominal yield strength (F_y) of 380 MPa. The length of the pin-ended members was 2380 mm, which corresponds to a slenderness ratio of 68. Ultra-high modulus unidirectional carbon fibre sheets were bonded to the specimens in the longitudinal direction. A single layer was 0.54 mm thick and had tensile strength and modulus of 510 MPa and 230 GPa, respectively. A layer of glass-FRP (GFRP) sheet was first installed directly on the steel surface before applying the CFRP layers to prevent direct contact between carbon fibres and steel, which could lead to galvanic corrosion. The GFRP lamina was 1.46 mm thick and had tensile strength and modulus of 855 MPa and 20.3 GPa, respectively. The stress-strain curves of steel, CFRP, and GFRP are illustrated in Fig. 1(b).

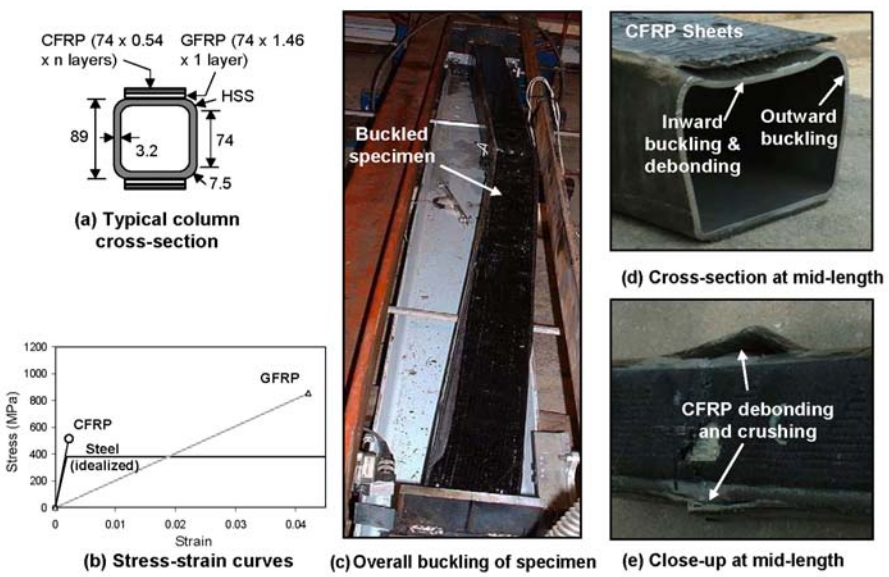

Fig. 1 Specimen cross-section, materials, test setup and failure mode

The tested specimens included a control (unretrofitted) specimen and three specimens retrofitted with one, three and five layers of CFRP, applied to two opposite sides in the plane of overall buckling. The fifth specimen was retrofitted with three layers, applied to all four sides of the specimen. The specimens were given identification codes. For example, 3L-2S indicates three CFRP layers applied on two opposite sides of the specimen.

The gain in axial strength of the FRP-retrofitted specimens ranged from 13 to 23 percent. The strength gains, however, did not correlate directly to the number of CFRP layers. As indicated earlier, this was attributed to the variability of geometric imperfections among the specimens, which is possibly due to a slight out of straightness of different values among the specimens, or minor misalignment within the test setup, or a combination of both. In all specimens, failure was mainly due to excessive overall bucking of the specimen, as shown in Fig. 1(c), followed by a secondary local buckling in the compression side, at or near mid length of the specimen. The local buckling took the form of inward buckling of the compression face and outward buckling of the two side faces, which was clearly revealed after testing by cutting the specimen, as shown in Fig. 1(d). For the FRP-retrofitted specimens, the secondary local buckling in the compression side was associated with a combined delamination and premature crushing of the FRP sheets. For specimen 3L-4S, retrofitted on four sides, the CFRP on the sides have also fractured due to the local bending associated with the outward buckling, as shown in Fig. 1(e).

Figure 2 shows the load versus axial strain of all specimens, at the two opposite sides, at mid-length. The figure shows that both sides are under compression, up to a certain load, where excessive buckling starts. At this load level, the strain readings at the outer surface revert to tension while strains at the inner surface show rapid increase in compression. The strain gauges on the compression side failed as a result of debonding and crushing of CFRP sheets. By carefully examining the strain readings, an average strain value of 0.0013 mm/mm can be defined as the strain at which CFRP failed in compression.

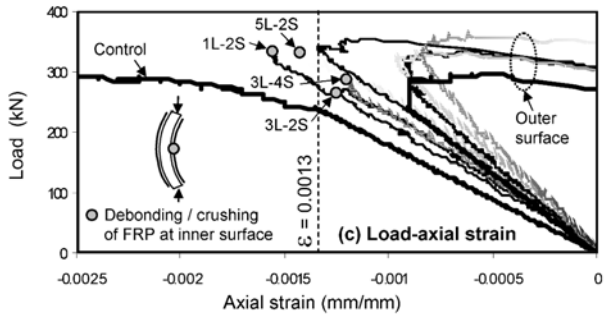

Fig. 2 Load-axial strain of experimental program

Analytical Model

In order to predict the load versus axial and lateral displacement responses of axially loaded slender HSS steel members retrofitted with CFRP sheets, a non-linear model has been developed. The model accounts for both material and geometric (second order effects) non-linearities as well as residual stresses. An incremental approach is used, where the concepts of equilibrium and strain compatibility are satisfied at each loading step. The stress-strain curve of steel is assumed to follow an elastic-perfectly plastic model, as shown in Fig. 1(b). On the other hand, FRP materials are assumed to behave linearly up to failure. The following sections provide detailed description of the model.

Residual Stresses in HSS Section

Residual stresses play an important role in the behaviour of steel structures and are normally induced in the manufacturing process. They typically result in a reduction of the flexural rigidity of slender members, and consequently, a lower buckling load may result (Weng, 1984). Although residual stresses are self-equilibrating, the cross sectional effective moment of inertia will be changed when parts of the section reach their yielding strength prior to other parts. An extensive experimental investigation of the residual stresses of hollow structural cold formed steel shapes was performed (Davison and Birkemoe, 1983 and Weng and Pekoz, 1990). The magnitudes of the measured residual stresses were found to vary, approximately, from 25 to 70 percent of the yield strength, depending on the manufacturing process.

Short columns are typically used in lieu of coupon tests to provide the average compressive stress-strain curves (Bjorhovde and Birkemoe, 1979). This type of tests demonstrates the overall column performance at very low slenderness ratio, in the absence of overall instability. The capacity of these columns is achieved when all fibres reach the yield stress and the corresponding load is defined as the yield load. Because of residual stresses, the short columns do not typically show a distinct yield point, but rather a gradual transition from the linear elastic behaviour to the fully plastic plateau, as a result of the gradual yielding. The magnitude of residual stresses F_{rs} can then be estimated by evaluating the difference between the proportional limit stress and the maximum stress levels. In this study, experimental short column tests have also been conducted by the authors on 175 mm long HSS columns of the same HSS sections used for the slender columns and the average load-strain curve is shown in Fig. 3. The behaviour shows a proportional limit load of 249 kN and a yield load of 410 kN. These two levels of load indicate that the magnitude of residual stress is in the order of 40 percent of the yield strength. In the proposed model, the through-thickness residual stress distribution will be idealized as shown in the schematic drawing in Fig. 3, as suggested by (Davison and Birkemoe, 1983) and by (Chan et al., 1991), where F_{rs} equals to the minimum value specified in literature as 0.25 F_y.

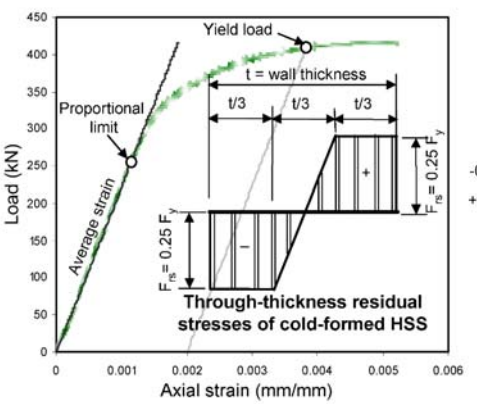

Fig. 3 Evaluation of residual stress magnitude

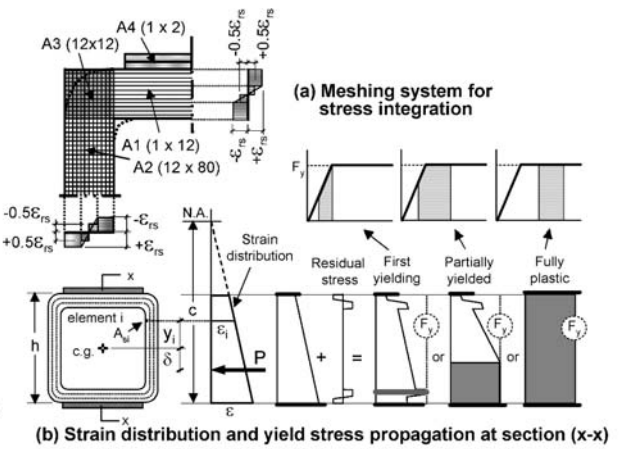

Fig. 4 Meshing system and yield propagation

In order to simulate the residual stress pattern, shown in Fig. 3, the wall thickness was first divided into three layers, as shown in Fig. 4(a). A pre-strain compressive value ε_{rs} of (-0.25 ε_y) was given to the inner third, while a tensile value of (+0.25 ε_y) was given to the outer third, where ε_y is the strain at yield, based on Fig. 1(b). The middle third was divided into two equal halves. The inner half was given a uniform value of (-0.125 ε_y), while the outer half was given a uniform value of (+0.125 ε_y), as shown in Fig. 4(a).

Meshing System

An element-by-element approach is adopted to integrate the stresses over the cross sectional areas of steel and FRP. The cross section was divided into four areas (A1 to A4), as shown in Fig. 4(a). The flat part of the flanges oriented normal to the plane of buckling (A1) was divided into 12 strips through the thickness, where the strain is constant across the width of each strip. The flat part of the flanges parallel to the plane of buckling (A2) was divided into 12 x 80 elements to capture the strain gradient along the depth of the section and also the residual stress distribution within the thickness. The conjunction between the flange and the web (A3) was idealized as a square and divided into 12 x 12 elements. Area A4 represents the FRP layers attached to area A1, and was divided into 1 x 2 elements. To model specimen 3L-4S with FRP sheets on four sides, an additional area of FRP, A5, attached to area A2, was also modeled. The distance between the center of each element and the centroid of the cross section is y_i, as shown in Fig. 4(b). It is assumed that perfect bond exists between the FRP sheets and steel

surface and strains are linearly distributed along the depth of the section. The stresses at the centroid of each element are assumed constant within the element area.

Force Equilibrium and Moments

Figure 4(b) shows a cross-section at mid-height of a concentrically loaded slender compression member. Due to overall buckling, the axial force is eccentric with respect to the mid-height section. For a given strain gradient induced by the external eccentric axial load *P*, which is based on a strain level ε at the extreme compression side and neutral axis depth *c*, the strain ε_i in each element *i* located at a distance y_i from the centroid can be determined as follows:

$$\varepsilon_i = \left[1 - \frac{h}{2c} - \frac{y_i}{c}\right]\varepsilon \tag{1}$$

where *h* is the depth of the section. The strain ε_i is then added to the residual strain ε_{rs} to obtain the total strain ε_{i+rs} for the steel elements and check whether the element has yielded or not:

$$\varepsilon_{i+rs} = \varepsilon_i + \varepsilon_{rs} \tag{2}$$

Possible stress distributions at various stages of loading are shown in Fig. 4(b). The total axial load at this loading level, for a given ε and *c*, can be obtained by numerical integration of stresses over the cross section, for both the yielded and elastic elements as well as the FRP elements, as follows:

$$P = \sum_{elastic\ steel}\left(\varepsilon_i\ E_s\ A_{s_i}\right) + \sum_{plastic\ steel}\left(F_y A_{s_i}\right) + \sum_{FRP}\left(\varepsilon_i\ E_f A_{f_i}\right) \tag{3}$$

and the corresponding moment *M* is:

$$M = \sum_{elastic\ steel}\left(\varepsilon_i\ E_s\ A_{s_i} y_i\right) + \sum_{plastic\ steel}\left(F_y A_{s_i} y_i\right) + \sum_{FRP}\left(\varepsilon_i\ E_f A_{f_i} y_i\right) \tag{4}$$

where A_{s_i} and A_{f_i} are the areas of steel and FRP elements, respectively, and E_{si} and E_{fi} are Young's moduli of steel and FRP elements, respectively.

Lateral Displacement

Figure 5(a) shows a pin-ended slender compression member which is slightly curved initially, due to an imperfection *e'*. At any load level *P*, the total lateral displacements, measured from the vertical axis is δ. (Allen and Bulson, 1980) have shown that the shape of the deflected compression member can be represented by a Fourier series, which can be reduced to the following expression that relates the lateral displacement δ at a distance *z* along the member's length to the applied load *P*:

$$\delta = \frac{e'}{1 - \left(P / P_{cr}\right)} \sin\left(\frac{\pi\ z}{L}\right) \tag{5}$$

where *L* is the length of member and P_{cr} is the Euler buckling load and is given by:

$$P_{cr} = \frac{\pi^2 EI}{(kL)^2} \tag{6}$$

where *EI* is the flexural rigidity of a prismatic member, function of Young's modulus *E* and moment of inertia *I* of the member's cross section. The effective length factor *k* accounts for boundary conditions and is taken as unity for pin-ended members.

It should be noted that Eq. 5 is valid for lateral displacements of value up to 10% of the length $(\delta \le L/10)$. It is also important to note that Equations 5 and 6 assume linear elastic behaviour of the material and that the residual stresses are not taken into consideration. In the following sections, methods are proposed to account for residual stresses, material non-linearity due to yielding, and the contribution of FRP.

Effective Moment of Inertia (I_{eff})

In order to account for gradual yielding of different parts of the cross section under the applied loading, the concept of "effective moment of inertia" is incorporated in this analysis. Contribution of any steel

element of area A_{s_i} to the flexural rigidity $(EI)_{s_i}$ is the product of the tangent modulus and the element's moment of inertia, as follows:

$$(EI)_{s_i} = E_t \; A_{s_i} \; y_i^2 \tag{7}$$

where E_t is the tangent modulus based on the stress-strain curve of steel. If the idealized elastic-plastic stress-strain curve of steel with Young's modulus E_s is used, then: for $\varepsilon_{i+rs} < \varepsilon_y$, $E_t = E_s$ and for $\varepsilon_{i+rs} \geq \varepsilon_y$, $E_t = 0$. This indicates that the flexural rigidity of the yielded parts becomes zero. Consequently, the effective bending stiffness $(EI)_{s_{eff}}$ of the entire section takes the following form:

$$(EI)_{s\,eff} = E_s \; . \sum_{elastic\ steel} \left(A_{s_i} \; y_i^2\right) \tag{8}$$

The effective moment of inertia $I_{s_{eff}}$ for the section can then be introduced in terms of the elastic parts only as follows:

$$I_{s\,eff} = \sum_{elastic\ steel} \left(A_{s_i} \; y_i^2\right) \tag{9}$$

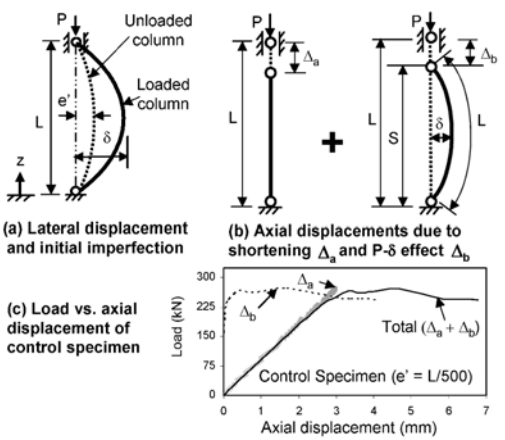

Fig. 5 Lateral and axial displacements of compression members

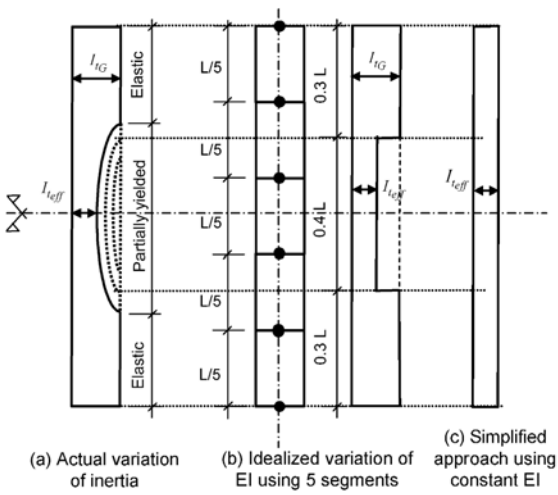

Fig. 6 Variation of stiffness (EI) along member's length due to yielding

First yielding will typically occur at the extreme fibres of the member's cross-section at mid-height. As the axial load and corresponding lateral deflection increase, yielding will spread within the cross-section and also in the longitudinal direction of the member, as shown in Figures 4(b) and 6(a). This indicates that the member will have a moment of inertia that varies with the applied load and also longitudinally within the yielded length as indicated by Eq. 9. As such, a more general expression for the Euler buckling load may be used in lieu of Eq. 6, which assumes a constant moment of inertia. The finite-difference method is used in this case (Ghali and Neville, 1989), where the member is divided into a number of segments of equal length λ and the equivalent concentrated elastic loads at each of the *m* internal nodes can be obtained. A series of simultaneous equations are then solved. The solution of these equations is an eigenvalue problem. An iteration procedure is utilized until a stable eigenvector {δ} is obtained. The buckling load P_{cr} can then be calculated from the largest eigenvalue γ as in Eq. 10. Figure 6(b) shows the idealized compression member and the variation of stiffness using five segments.

$$\gamma = \frac{12}{P_{cr}\,\lambda^2} \tag{10}$$

A conservative yet reliable simplification may be made by assuming that flexural stiffness of the critical section at mid-height (using Eq. 9) governs, and can then be assumed constant along the length of the member, as shown in Fig. 6(c). This will allow the use of the simple Euler buckling formula, as shown in Eq. 11.

$$P_{cr} = \frac{\pi^2 E_s I_{s\,eff}}{(kL)^2} \tag{11}$$

For HSS sections with FRP layers, the transformed effective moment of inertia $I_{t_{eff}}$ should be used in lieu of $I_{s_{eff}}$ in Eq. 11. $I_{t_{eff}}$ is calculated using the following equation:

$$I_{t_{eff}} = I_{s\,eff} + \sum_{FRP}\left[\frac{E_{f_i}}{E_s} I_{f_i}\right] \tag{12}$$

where $I_{f_i} = \left(A_{f_i}\ y_i^2\right)$. I_{fi}, E_{fi} and A_{fi} are the moment of inertia, Young's modulus, and the area of intact FRP element *i*, respectively.

The lateral displacement of the member can now be calculated at any point along the member's length, at any load level, using Eq. 5.

Axial Displacement

The axial displacement Δ is the sum of two components, Δ_a and Δ_b, as shown in Fig. 5(b):

$$\Delta = \Delta_a + \Delta_b \tag{13}$$

where Δ_a and Δ_b are the displacements due to axial shortening and curvature arising from P-δ effect, respectively, and can be approximated as follows:

$$\Delta_a = \frac{PL}{E_s A_t} \tag{14}$$

where A_t is the transformed cross sectional area and is calculated as follows:

$$A_t = A_s + \sum_{FRP}\left[\frac{E_{f_i}}{E_s} A_{f_i}\right] \tag{15}$$

where, A_s is the cross sectional area of the HSS section

$$\Delta_b = L - S \tag{16}$$

where S is the chord length of the deformed shape of the compressed member (Fig. 5(b)), and is calculated based on a sine curve of arc length L and amplitude δ for the member's deflected shape.

Figure 5(c) shows the predicted load-axial displacement response of the control specimen. The figure shows that the contribution of the 'curvature' component Δ_b is only significant near and after the peak load, where the overall buckling occurs, whereas the axial shortening component Δ_a is dominant within the linear elastic range, before buckling.

Failure Criteria

The strain values in the steel cross section are incrementally increased, until the section reaches its full plastic capacity, as shown in Fig. 4(b). Elements with compressive residual stresses typically reach yielding before elements with tensile residual stresses. Eventually, all elements reach the yield strength. At this point, the effective moment of inertia of the steel cross section and the buckling load become zero, based on Equations 9 and 10. Consequently, a value for the lateral displacement δ can no longer be obtained using Eq. 5.

For FRP material in the compression side, the failure strains are limited by debonding and crushing at a strain value of 0.0013 mm/mm. After excessive overall buckling, the FRP on the outer surface may be subjected to some tensile strains, which are well below the ultimate value.

Generation of Full Responses

In order to obtain the load-lateral displacement (P-δ) response in compression, the procedure can be summarized as follows:

1. Assume a value of the extreme compressive strain ε and a neutral axis depth c (Fig. 4(b)).
2. For each element of the steel cross section, calculate its strain value ε_i, using Eq. 1, add the residual strain ε_{rs} as given by Eq. 2, and compare it to the yield strain value ε_y to check whether the element has yielded or not.
3. Calculate the corresponding stress of each element, using the steel stress-strain curve. For $\varepsilon_{i+rs} \geq \varepsilon_y$, the stress is limited to F_y.
4. Calculate the strain ε_i, using Eq. 1, and corresponding stress for each FRP element, based on linear stress-strain response. Compare the strain to ultimate values to check for failure of FRP.
5. Calculate the axial load P and bending moment M for the entire cross section, by using Equations 3 and 4, which are essentially a summary of steps 3 to 5 above.
6. Calculate the eccentricity $e = M/P$, which is induced by the non uniform stress distribution.
7. Calculate the cross sectional transformed effective inertia $I_{t_{eff}}$, excluding both the yielded steel elements and failed FRP elements, using Eq. 12.
8. Calculate the critical load P_{cr} using the conservative approach described by Eq. 11 (or alternatively using the more accurate approach by using Eq. 10). P_{cr} is used to calculate the lateral displacement at mid-length δ for a prescribed imperfection e' using Eq. 5.
9. Compare the eccentricity e obtained in step 6 with the lateral displacement δ, calculated in step 8. If the two values are different, assume a new value of the neutral axis depth c and repeat steps 2 to 8 until the two values are equal. This will provide one point on the load-lateral displacement curve.
10. Enter a higher value of strain ε in step 1 and repeat the process from steps 2 to 9 until the complete load-lateral displacement response is established.

In order to generate an approximate load-axial displacement P-Δ response of compression members, for an axial load P and corresponding lateral deflection δ, obtained earlier, the following procedure can be followed:

1. The axial shortening term Δ_a of the displacement is calculated using Eq. 14.
2. For a given lateral displacement δ, establish the deformed sine curve of a buckled member with mid-length amplitude of δ and an arc length of L.
3. Calculate the chord length of the sine curve S.
4. Calculate the 'curvature' component of the axial displacement Δ_b using Eq. 16.
5. The total axial displacement Δ is calculated using Eq. 13.
6. Repeat the previous steps for each load level P and its corresponding lateral displacement δ, until the complete P-Δ response is established.

Verification of Model and Parametric Study

The model described in the previous section has included several features, namely the P-δ effect (non-linear geometry), plasticity (yielding) of the steel section, the through-thickness residual stresses in the HSS section, the initial imperfection, and failure criteria of FRP in compression. In order to illustrate the significance of these features, the load-lateral displacement response of one specimen retrofitted with three CFRP layers, on two opposite sides, (3L-2S) has been predicted for five different cases. In case 1, Equations 5 and 6 have been used in their original form, assuming linear elastic materials (ignoring steel yielding and residual stresses). In case 2, plasticity of steel is considered, however, residual stresses are ignored. In case 3, both steel plasticity and residual stresses are accounted for but the failure criteria of FRP in compression is not applied (FRP is assumed fully intact in the compression side throughout the full response). In case 4, all the features of the model are applied, including the effect of variable inertia along the length, which is accounted for in calculating the buckling load, using the finite difference approach as shown in Fig. 6(b). Case 5 is similar to case 4, except that the simplified approach for calculating the buckling load is used, as shown in Fig. 6(c).

Figure 7 shows the experimental and analytical responses for the five cases. All predictions were made assuming initial imperfection ($e' = L/500$), which is the limit permitted by Canadian standards (CAN/CSA-S16-01). The effect of initial imperfection itself will be discussed later. Figure 7 clearly shows that ignoring the steel plasticity (case 1) would highly over estimate the axial strength. Ignoring the residual stresses (case 2) would also overestimate the load at which transition occurs from the elastic to plastic response. Also by assuming that FRP is fully effective in compression (case 3), the ultimate load is somewhat overestimated. It is, therefore, clear that cases 4 and 5 represent the most accurate predictions, using the full capabilities of the model. It is also clear that the simplified conservative approach used in case 5 is quite reasonable and would, therefore, be used in this paper for the predictions of all responses and the parametric study, next.

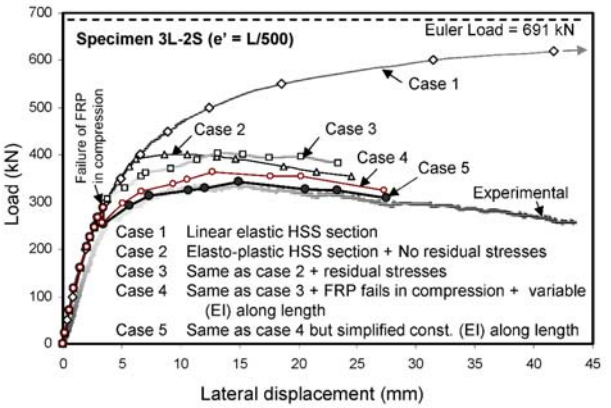

Fig. 7 Significance of various features of analytical model

The load versus lateral and axial displacements of the five specimens have been predicted and are presented in Figures 8(a) and 8(b), respectively. A summary of the predicted and experimental values is also presented in Table 1. The predictions are made for three different levels of initial imperfections, namely $L/300$, $L/500$, and $L/1000$. It is expected that most steel sections will practically have imperfection values less than $L/500$ (CAN/CSA-S16-01). The model shows reasonable agreement with test results for this common level of imperfections. However, for specimen 5L-2S, the behaviour was not accurately predicted since the maximum lateral displacement, measured experimentally, occurred near the quarter length point, rather than at mid-length. Also, for the same reason, this specimen did not show higher gain of strength compared to other specimens, with less number of CFRP layers. Figures 8(a) and 8(b) clearly emphasize the important effect of initial imperfection. The load-axial strain behaviour at two opposite sides of each specimen has also been predicted in Fig. 8(c), using the imperfection value that showed the best results for each respective specimen.

It has been shown that the model is capable of predicting the various responses of axially loaded slender HSS members retrofitted with CFRP sheets. It was also shown earlier, in the experimental results, that no clear correlation was established between the number of CFRP layers and strength gains, due to the variability of imperfections among the test specimens. In the following section, the model is used to study the sole effect of the number of CFRP layers, by fixing the level of imperfection. This study builds on the same specimens used to verify the model. The responses of control, 1L-2S, 3L-2S, and 5L-2S specimens are estimated twice, using two fixed values of imperfections, namely $L/300$ and $L/1000$, as shown in Fig. 9.

Effect of Number of CFRP Layers

Figure 9 (a and b) clearly shows that bonding CFRP sheets to slender HSS members can indeed increase their axial compressive strength. For example, the predicted percentage increases in strength of specimens with one, three and five CFRP layers are 11, 25, and 40 percent for specimens with $L/300$ imperfection and are 12, 26, and 40 percent, respectively, for specimens with $L/1000$ imperfection.

Also, the percentage increases in axial stiffness are 15, 31, and 48 percent for the *L*/300 specimens and are 13, 29, and 45 percent, for the *L*/1000 specimens. These findings show that the percentage increases in axial strength and axial stiffness, for the levels of imperfections studied, are independent of the initial imperfection value. The imperfection, however, affects the absolute values of ultimate loads.

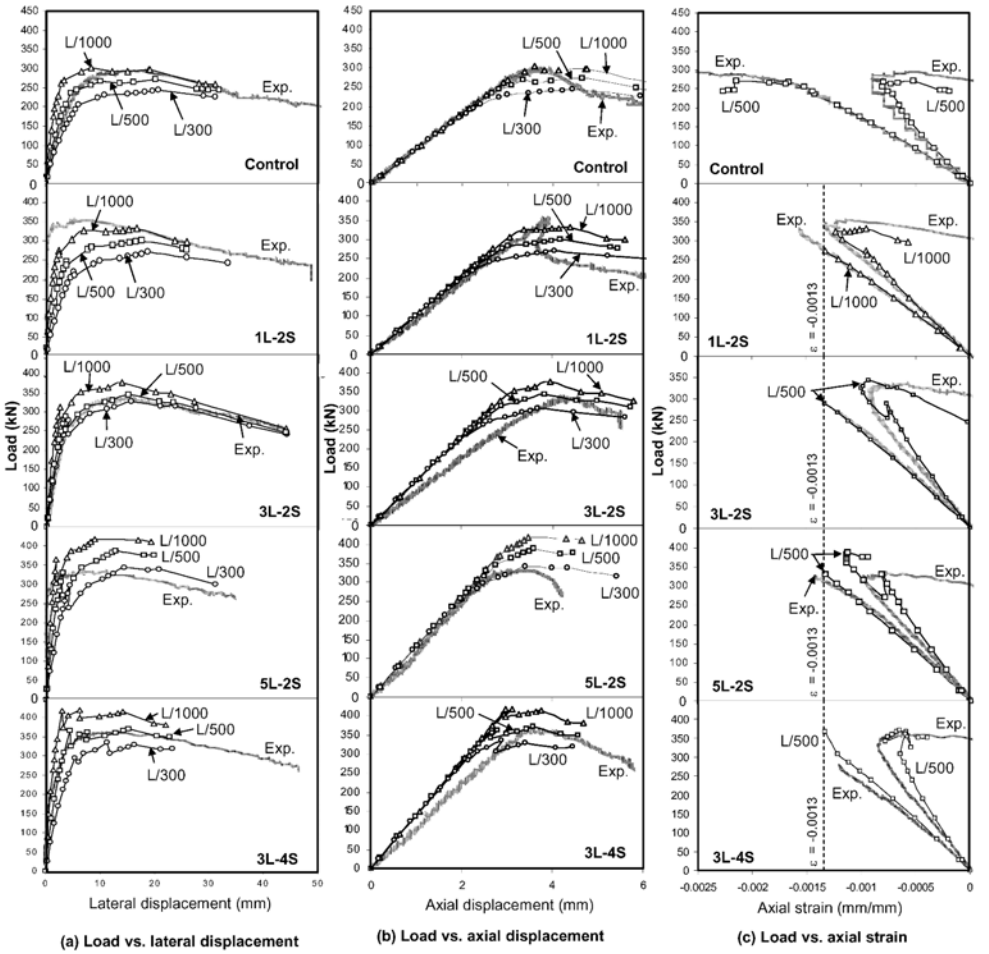

Fig. 8 Predicted responses of the slender HSS compression members

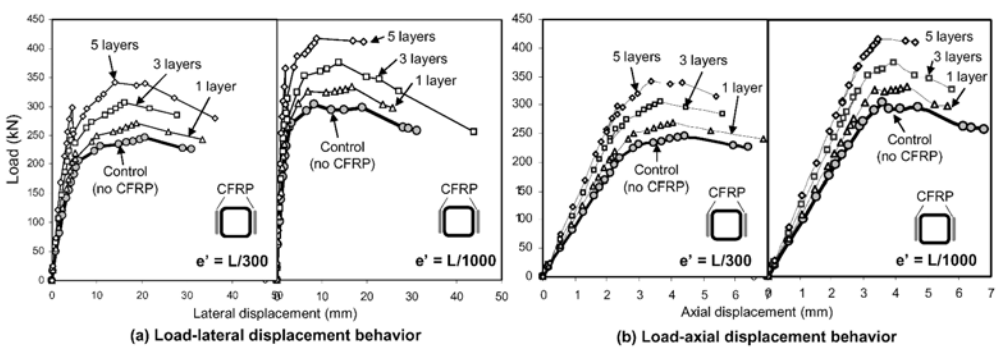

Fig. 9 Effect of number of CFRP layers on behavior of HSS compression members

Table 1. Comparison between experimental and analytical model results

Experimental		Analytical Model		(Analytical / Experimental) ratio
Specimen I.D.	P_{max} (kN)	e'	P_{max} (kN)	
Control	295	L/300	245	0.83
		L/500	271	0.92
		L/1000	297	1.01
1L-2S	355	L/300	271	0.76
		L/500	301	0.85
		L/1000	333	0.94
3L-2S	335	L/300	306	0.91
		L/500	344	1.03
		L/1000	375	1.12
5L-2S	332	L/300	344	1.04
		L/500	387	1.17
		L/1000	415	1.25
3L-4S	362	L/300	329	0.91
		L/500	371	1.02
		L/1000	415	1.15

Table 2. Percentage increases in axial strength and stiffness of retrofitted members

Imperfection value (e')	Specimen I.D.	P_{max} (kN.)	% Gain in strength	Axial Stiffness (kN/mm)	% Gain in stiffness
L/300	control	245	-	89	-
	1L-2S	271	11	102	15
	3L-2S	306	25	117	31
	5L-2S	344	40	132	48
L/500	control	271	-	91	-
	1L-2S	301	11	103	13
	3L-2S	344	27	117	29
	5L-2S	387	43	132	45
L/1000	control	297	-	91	-
	1L-2S	333	12	103	13
	3L-2S	375	26	117	29
	5L-2S	415	40	132	45

Conclusions

A non-linear model based on the concepts of equilibrium and strain compatibility has been developed to predict the axial load capacity of slender HSS compression members retrofitted by externally bonded CFRP sheets. The model is also capable of predicting the full load versus lateral and axial displacements. The member's initial imperfection, residual stresses, material and geometric nonlinearities are accounted for. The model was verified using experimental results and showed reasonable agreement. The effects of member's initial imperfection and number of CFRP layers are studied. The following conclusions can be drawn, based on the simplified conservative approach followed, and the range of imperfections studied in this paper:

1. Externally bonded CFRP sheets are effective in increasing the axial strength and stiffness of slender HSS compression members.
2. For a slender member retrofitted by a given CFRP reinforcement ratio, the member's initial imperfection has a pronounced effect on its axial strength but marginal effect on axial stiffness.
3. While initial imperfection affects the magnitude of member's axial strength, it does not affect the percentage increase in member's strength resulting from CFRP retrofitting, for the studied level of imperfections.
4. Ignoring residual stresses, steel plasticity, or premature delamination and crushing of CFRP in the inward side of a compression member undergoing overall buckling could highly overestimate the member's axial strength.

Future Work

The model will be further refined to account for the effect of the variable inertia throughout the length of the column by introducing larger number of segments.

Acknowledgement

The authors wish to acknowledge the financial support provided by the Natural Sciences and Engineering Research Council of Canada (NSERC).

References

1. Allen, H. G. and Bulson, P. S. (1980). "Background to Buckling." McGraw-Hill Book Company (UK) Limited.S.
2. Bjorhovde, R., and Birkemoe, P. C. (1979). "Limit States Design of HSS Columns." Canadian Journal of Civil Engineering, 6, 275-291.
3. Canadian Standards Association, CAN/CSA-S16-01, Limit states design of steel structures, Mississauga, Ontario.
4. Chan, S. L., Kitipornchai, S. and Al-Bermani, F. G. A. (1991). "Elasto-Plastic Analysis of Box-Columns including Local Buckling Effects." Journal of Structural Engineering. ASCE, 117(7): 1946-1962.
5. Davison, T. A., and Birkemoe, P. C. (1983) "Column Behaviour of Cold-Formed Hollow Structural Steel Shapes." Canadian Journal of Civil Engineering, 10, 125-141.
6. Ghali, A. and Neville, A. M. (1989). "Structural analysis: A unified classical and matrix approach" Chapman and Hall, London and New York.
7. Hollaway, L.C. and Cadei, J. (2002). "Progress in the Technique of Upgrading Metallic Structures with Advanced Polymer Composites", Progress in Structural Engineering and Materials, J. Wiley & Sons, 4(2):131-148.
8. Shaat, A., Schnerch, D., Fam, A., and Rizkalla, S. (2004) "Retrofit of steel structures using fiber-reinforced polymers (FRP): State-of-the-art.", Transportation Research Board (TRB) Annual Meeting, Washington, D.C., USA, CD-ROM (04-4063).
9. Shaat, A. and Fam, A. (2006) "Axial Loading Tests on CFRP-Retrofitted Short and Long HSS Steel Columns." Accepted for publication in the Canadian Journal of Civil Engineering.
10. Weng, C. C. (1984). "Cold-bending of thick steel plates at low R/t ratios." Master's thesis. Cornell University, at Ithaca, N.Y.
11. Weng, C. C., and Pekoz, T. (1990). "Residual Stresses in Cold-Formed Steel Members." Journal of Structural Engineering. ASCE, 116(6): 1611-1625.